Supplementary Information for

Molecular dynamics study of thermal transport in dinaphtho[2,3-b:2',3'-f]thieno[3,2-b]thiophene (DNTT) organic semiconductor

Xinyu Wang,[a] Jingchao Zhang,[b] Yue Chen*[a] and Paddy K. L. Chan*[a]

[a] Department of Mechanical Engineering, The University of Hong Kong, Hong Kong

[b] Holland Computing Center, University of Nebraska-Lincoln, Lincoln, NE 68588, USA

1. Potential parameters in the simulation

In the simulation, the general AMBER force field (GAFF)[1] is employed to describe the intermolecular and intramolecular interactions of DNTT molecules. According to GAFF, the total energy of the system, E_{pair}, includes five components: the bond, angle, dihedral, van der Waals interaction (Lennard-Jones potential) and electrostatic terms, as presented below:

$$E_{pair} = \sum_{bonds} k_r \left(r - r_{eq}\right)^2 + \sum_{angles} k_\theta \left(\theta - \theta_{eq}\right)^2 + \sum_{dihedrals} \frac{v_n}{2} \times \left[1 + \cos\left(n\varphi - \gamma\right)\right] + \sum_{i<j} 4\varepsilon \left[\left(\frac{\sigma}{R_{ij}}\right)^{12} - \left(\frac{\sigma}{R_{ij}}\right)^{6}\right] + \sum_{i<j} C \frac{q_i q_j}{R_{ij}} \quad \text{(S1)}$$

where, r and θ are the bond length and angle, respectively; subscript "*eq*" is the equilibrium condition; k_r, k_θ and v_n are force constants; n is multiplicity and γ is phase angle for torsional angle parameters; R is the distance between atoms; ε is the depth of potential well; σ is the zero energy separation distance; C is an energy-conversion constant; subscript "q" is the charge; subscript "i" and "j" represent atoms. The cutoff distances for van der Waals interaction and electrostatic terms are 10 Å. The detailed GAFF parameters used in the simulation are shown as follows.

* Corresponding authors. E-mail: pklc@hku.hk (Paddy K. L. Chan) and yuechen@hku.hk (Yue Chen).

Table S1 List of atom types

Atom	Type	Description
Carbon	CA	Aromatic carbon
	CB	Aromatic carbon at junction of 5- and 6-membered rings and attached to sulfur
	CC	Aromatic carbon at junction of 5- and 6-membered rings and unattached to sulfur
	CS	Carbon at junction of two 5-membered rings
Hydrogen	H	H attached to aromatic carbon
Sulfur	S	Sulfur in 5-membered ring

Table S2 List of bond parameters

Bond	k_r (kcal/mol-Å^2)	r_{eq} (Å)
CA-CA	461.8814	1.3980
CA-CB	491.2172	1.3790
CA-CC	503.4213	1.3715
CA-H	354.4883	1.0800
CB-CC	415.8478	1.4310
CB-S	281.1149	1.7345
CS-CC	415.8478	1.4310
CS-CS	524.5962	1.3590
CS-S	281.1149	1.7345

Table S3 List of angle parameters

Angle	k_θ (kcal/mol-rad^2)	r_{eq} (°)
CA-CA-CA	66.2729	120.3300
CA-CA-CB	67.4806	119.6500
CA-CA-CC	66.3204	120.8500
CA-CA-H	48.4896	119.6600
CB-CA-H	48.5895	120.2000
CC-CA-H	49.2921	119.6000
CA-CB-CC	65.1698	121.0000
CA-CB-S	57.1273	126.1000
CC-CB-S	52.0963	132.2500
CA-CC-CB	67.0927	119.4000
CA-CC-CS	67.0927	119.4000
CB-CC-CS	78.5432	109.2500
CC-CS-CS	73.8973	114.0000
CC-CS-S	52.0963	132.2500
CS-CS-S	70.6060	113.6000
CB-S-CS	102.6176	90.2800

Table S4 List of dihedral angle parameters

Angle	$\frac{v_n}{2}$ (kcal/mol)	n	γ (°)
X-CA-CA-X	3.6250	2	180
X-CA-CB-X	3.5000	2	180
X-CA-CC-X	3.5000	2	180
X-CB-CC-X	5.4500	2	180
X-CB-S-X	0.3333	3	0
X-CC-CS-X	1.6750	2	180

X-CS-CS-X	6.6500	2	180
X-CS-S-X	0.3333	3	0

Table S5 List of improper dihedral angle parameters

Angle	$\frac{v_n}{2}$ (kcal/mol)	n	γ (°)
X-X-X-X	1.1	2	180

Table S6 List of Lennard-Jones potential parameters

Atom type	ε (kcal/mol)	σ (Å)
CA	0.0860	3.4000
CB	0.0860	3.4000
CC	0.0860	3.4000
CS	0.0860	3.4000
H	0.0150	2.6000
S	0.2500	3.5640

Table S7 List of charge parameters

Atom type	q
CA (attached to H)	-0.1270
CA (unattached to H)	0.0000
CB	-0.0130
CC	0.0000
CS	-0.0130
H	0.1270
S	0.0260

2. Definition of actual heat transport directions of the simulation box (a^*, b^* and c^*)

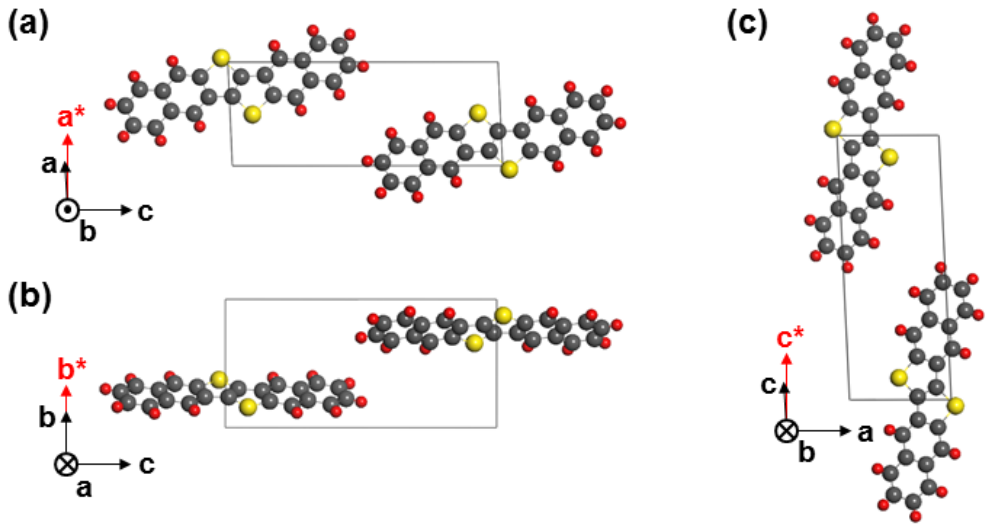

Fig. S1 Definition of actual heat transport directions of the simulation box. (a) for a^*, (b) for b^* and (c) for c^*.

3. Effect of simulation boundary condition along heat transport direction on thermal conductivity of 50 nm DNTT thin film (c^* direction)

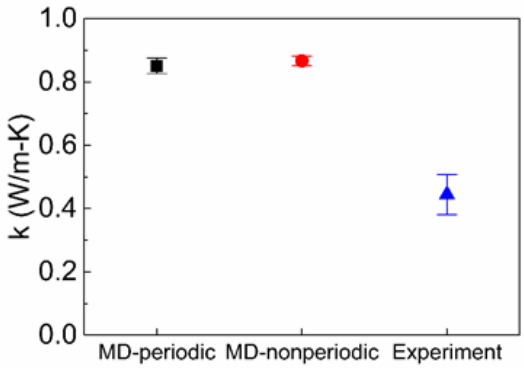

Fig. S2 Thermal conductivity of 50 nm DNTT thin film (c^* direction) simulated by MD simulations and experimental measurement. MD-periodic represents the periodic boundary condition is applied along heat transport direction in the simulation, MD-non-periodic represents the free boundary condition is applied along heat transport direction in the simulation. It can be noted that there is no significant difference between the periodic and non-periodic MD results of DNTT thermal conductivity.

4. Thermal rectification calculation for different DNTT crystal boundaries

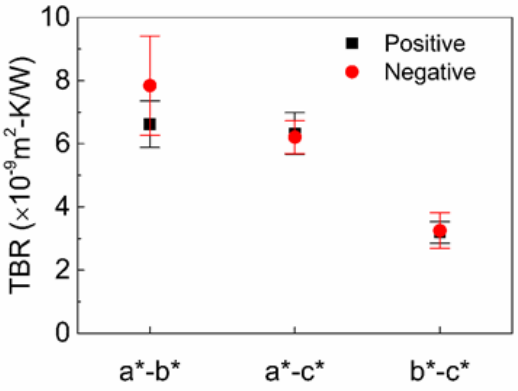

Fig. S3 Thermal rectification calculation for different DNTT crystal boundaries. By changing the location of heat source and sink, it can create positive and negative heat transport directions. No thermal rectification phenomenon is observed.

5. Heat flux distribution for different DNTT crystal boundaries

To further get insights in the effect of crystal boundary, we calculate the spatial distribution of heat flux for different DNTT crystal boundaries (a^* - b^*, a^* - c^* and b^* - c^* interfaces). To obtain the atomic heat flux, the system firstly arrives at the steady state in the NEMD process. The atomic heat flux is calculated by the following expression: $\boldsymbol{J}_i = \boldsymbol{e}_i \cdot \boldsymbol{v}_i + \boldsymbol{S}_i \cdot \boldsymbol{v}_i$, where the subscript "$i$" is the atom, $\boldsymbol{J}$ is atomic heat flux, $\boldsymbol{e}$ is energy of atom, $\boldsymbol{v}$ is the velocity, and $\boldsymbol{S}$ is the stress.[2] The final atomic heat flux distribution is averaged during 10 ps in the steady state of NEMD. Fig. S4 shows the heat flux distribution for a^* - b^*, a^* - c^* and b^* - c^* interfaces. In comparison with interface structures of Fig. 5, we can observe that there the strong scatterings of heat flux around the interface regions.

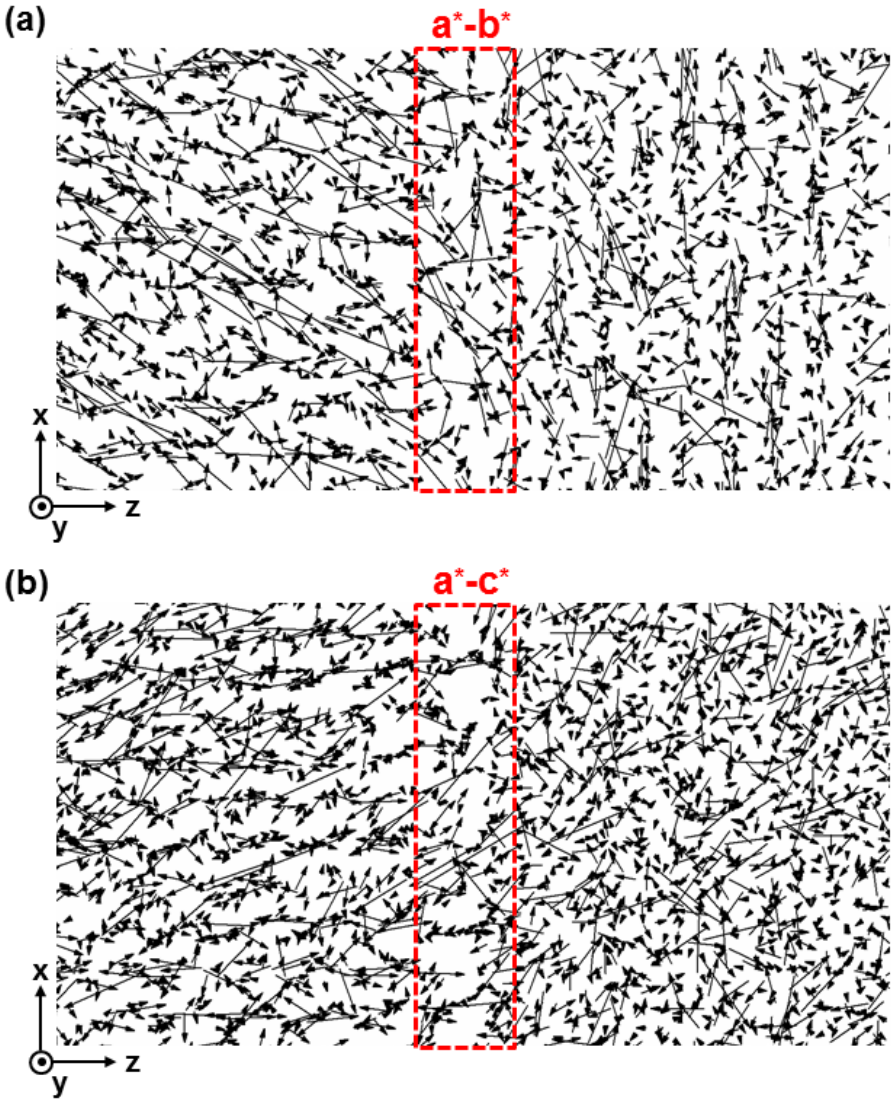

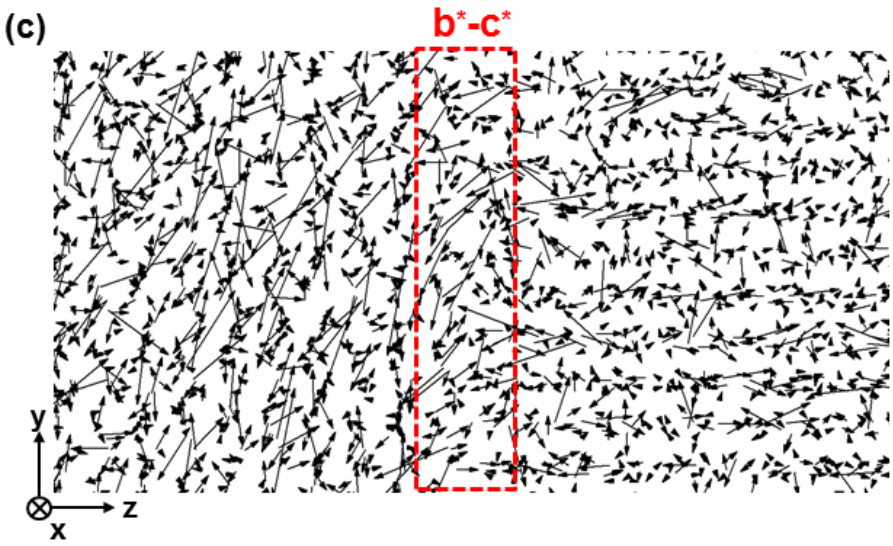

Fig. S4 Heat flux distribution for different DNTT crystal boundaries. (a) for a^* - b^* interface, (b) for a^* - c^* interface, and (c) for b^* - c^* interface. The red rectangular boxes represent the interface regions.

6. Heat flux distribution for different DNTT crystal orientations with vacancy

We also calculate the spatial distribution of heat flux for different DNTT crystal orientations with 6% vacancy concentration as shown in Fig. S5. It can be noted that the vacancies appear in the system as the red circles show. There exists the scattering of heat flux around the vacancy regions, which further confirms the effect of vacancy on the thermal conductivity.

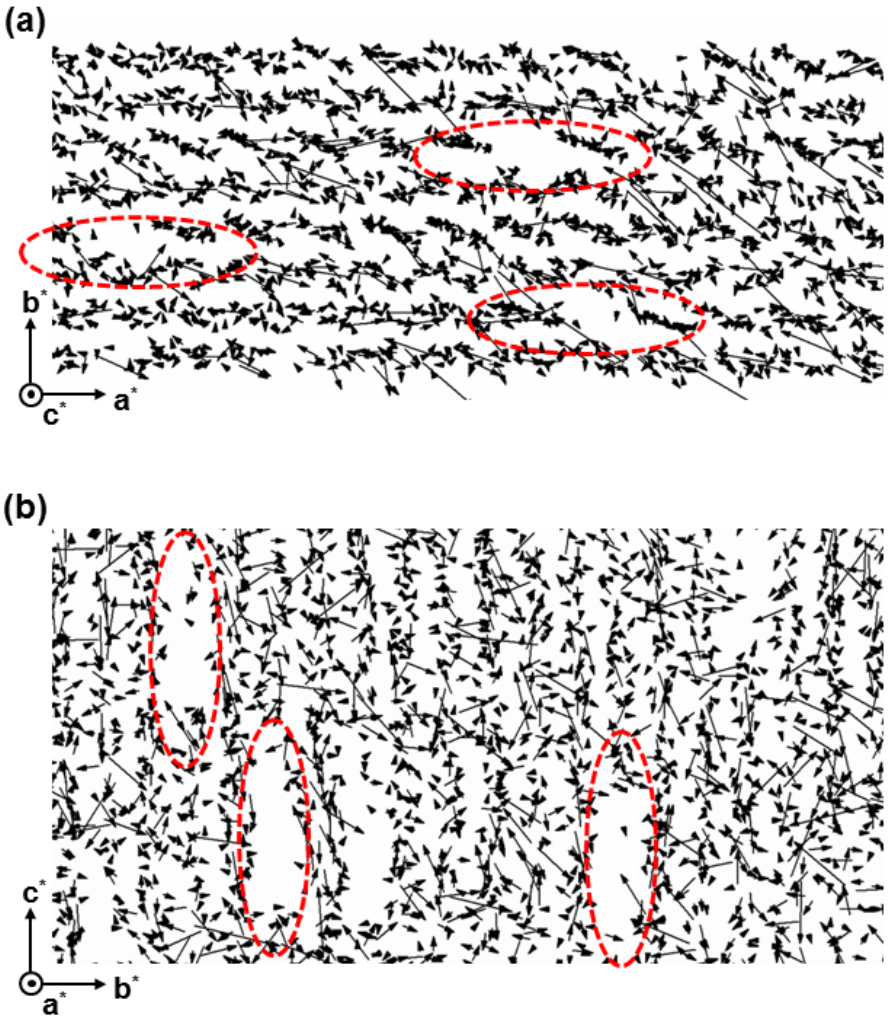

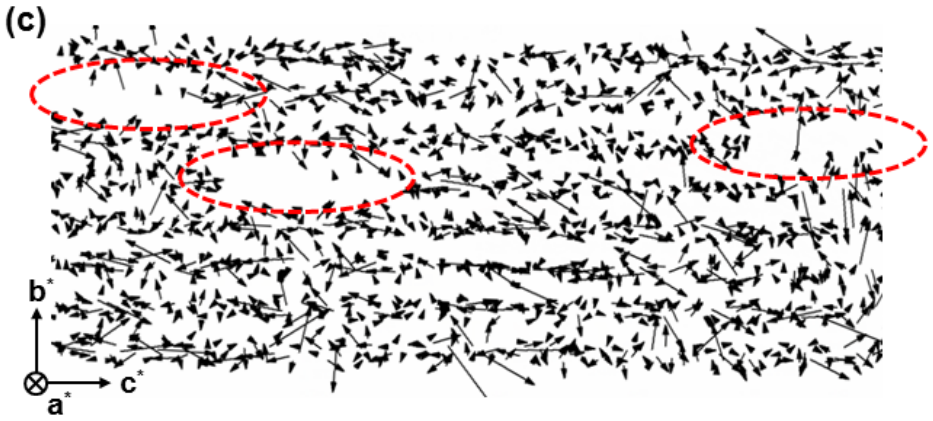

Fig. S5 Heat flux distribution for different DNTT crystal orientations with 6% vacancy concentration. (a) for a^* direction, (b) for b^* direction, and (c) for c^* direction. The red circles represent the vacancy regions.

References

1. J. Wang, R. M. Wolf, J. W. Caldwell, P. A. Kollman and D. A. Case, *J. Comput. Chem.*, 2004, **25**, 1157-1174.
2. Y. Wang, Z. Song and Z. Xu, *J. Mater. Res.*, 2014, **29**, 362-372.